Composites Part B 93 (2016) 43–55

Contents lists available at ScienceDirect

Composites Part B

journal homepage: www.elsevier.com/locate/compositesb

# Study on the mechanical and drilling properties of AA7039 composites reinforced with $Al_2O_3/B_4C/SiC$ particles

Şener Karabulut [a, *], Uğur Gökmen [b], Henifi Çinici [c]

[a] Department of Mechanical Program, Hacettepe University, 06935 Ankara, Turkey
[b] Technical Sciences Vocational School, Gazi University, 06500 Ankara, Turkey
[c] Department of Metallurgy and Materials Eng., Gazi University, 06500 Ankara, Turkey

ARTICLE INFO

*Article history:*
Received 14 December 2015
Received in revised form
1 February 2016
Accepted 24 February 2016
Available online 3 March 2016

*Keywords:*
A. Metal-matrix composites (MMCs)
B. Mechanical properties
B. Surface properties
E. Machining
Drilling

ABSTRACT

The hardness, transverse rupture strength (TRS), and elongation behavior of aluminum alloy 7039 (AA7039) reinforced with particulates of aluminum oxide ($Al_2O_3$), boron carbide ($B_4C$), and silicon carbide (SiC) were investigated to elucidate the effect of reinforcement content on the mechanical and drilling properties of the resulting composites. AA7039 and three composite specimens reinforced with 10 wt.% $Al_2O_3$, 10 wt.% $B_4C$, and 10 wt.% SiC were successfully produced using a powder metallurgy and hot-extrusion method. The samples of AA7039 and the composites were tested for hardness, TRS, elongation, and drilling behavior. The results revealed that the $Al_2O_3$, $B_4C$, and SiC reinforcement particulates were uniformly distributed in the matrix structure and that good interfacial bonding was achieved between the matrix and reinforcement elements. AA7039 composite reinforced with 10 wt.% $Al_2O_3$ exhibited the highest hardness, bending strength, and elongation among the investigated specimens. Fracture surface analysis revealed cracks in the fracture surface of AA7039/$B_4C$ and AA7039/SiC; these cracks propagated through the particle–matrix interfaces. The $Al_2O_3$-reinforced composite exhibited better interfacial bonding compared with the $B_4C$- and SiC-reinforced composites. Excellent surface quality was achieved in the drilling of the AA7039/$Al_2O_3$ composite specimen. Surface quality was improved at lower feed rates and decreased with increasing feed rate in the drilling of all specimens. Chip formation was affected by the mechanical and microstructural properties of the workpiece materials.



## 1. Introduction

Aluminum alloys (AAs) are desirable materials for numerous engineering implementations because of their excellent low-temperature properties, high strength-to-weight ratio, and good corrosion resistance. However, the main problem with AAs is their poor wear resistance and poor endurance to high temperatures. To solve these problems, researchers have been reinforcing AAs with ceramic particles; consequently, the number of reported investigations on metal–matrix composites (MMCs) is consistently increasing [1–3]. AA-based MMCs reinforced with ceramic particles exhibit enhanced mechanical properties compared with those of unreinforced AAs. Studies in recent years have indicated that MMCs are attractive engineering materials in many applications because of their superior mechanical properties and various benefits in applications such as nuclear power plants, armor, automobile parts, marine components, and aerospace parts. Aluminum oxide ($Al_2O_3$), boron carbide ($B_4C$), and silicon carbide (SiC) particles are extremely hard reinforcement elements with excellent mechanical properties; they are widely used in aluminum-based MMCs as reinforcement materials [4,5]. Ibrahim et al. [6] investigated the heat treatment conditions on the mechanical and fracture properties of an aluminum-based MMC reinforced with 15 vol.% $B_4C$. For this purpose, three aluminum 6063 based metal matrix composites were produced using the molten metal processing method for the experimental study. $B_4C$ particles were injected using powder injection apparatus into molten aluminum. Then, specimens were homogenized at the elevated temperatures for 48 h. In addition to this, all composites were quenched in warm water and aged in the range of 25–400 °C for 10 h, at each temperature. Hardness, tensile and fracture tests were performed on three MMCs. The authors achieved a uniform particle distribution and strong bonding with

* Corresponding author. Tel.: +90 312 267 30 20; fax: +90 312 267 33 38.
*E-mail address:* senerkarabulut@hacettepe.edu.tr (Ş. Karabulut).

http://dx.doi.org/10.1016/j.compositesb.2016.02.054
1359-8368/

the aluminum matrix. The hardness and strength of the resulting composites were increased after an aging process compared with those of pure aluminum. They also reported that $B_4C$ particles were retained in the matrix after the fracture due to protective layers of Zr/Ti and observed a cleavage mechanism on the surface of the fractured $B_4C$ particles. In another study, Ibrahim et al. [7] studied the impact toughness of Al–15 vol.% $B_4C$ MMCs. Ten specimens were fabricated and prepared as described in the previous study [6] adding small amount of Ti, Zr and Sc using a new powder injection technique. The microstructure and fracture surface results of the composite materials revealed that the presence of Ti improved the wettability of $B_4C$ particles in the matrix structure. The impact toughness of Al-based MMCs exhibited better toughness compared with Al 6063 reinforced with $B_4C$ composites, and the amount of the precipitated phases was the most significant parameter governing the composite toughness. Baradeswaran and Perumal [8] studied the effect of $Al_2O_3$ and graphite particle content on the mechanical and wear properties of AA7075-based hybrid composites. The composite specimens were produced using liquid metallurgy route by the addition of 5 wt.% graphite and subjected to T6 heat treatment. The wear, hardness, tensile strength, compressive strength and flexural strength of the composites were investigated. They reported that the tensile strength, flexural strength, hardness, and compression strength of the $Al_2O_3$/graphite-reinforced AA7075 hybrid composites increased with the weight percentage of the ceramic phase. Doel and Bowen [9] reported that an AA7075/SiC composite exhibited enhanced tensile strength and lower ductility compared with the unreinforced AA. Srivatsan [10] studied the effect of $Al_2O_3$ particles on the tensile deformation and fracture behavior of AA2014. The results showed that the elastic modulus and tensile strength of the MMC improved with increasing reinforcement content in the metal matrix. However, cracks and decohesion at the interfaces also increased with the content of reinforcing material in the matrix. Shorowordi et al. [11] performed a comparative study on the microstructure and interface characteristics of $Al_2O_3$-, SiC-, and $B_4C$-reinforced Al matrix composites. They observed that Al/$B_4C$ composites exhibited better particle dispersion and interfacial bonding than the other two composites. Rajkumar et al. [12] manufactured Al–$B_4C$ composites with $B_4C$ contents ranging from 5% to 15% using a stir-casting method and studied the mechanical and machinability characteristics of the composites in a turning machine. The impact toughness decreased and the hardness increased with increasing reinforcement content. The cutting force was decreased at higher machining speeds and increased at greater depth of cutting during the turning of the composites. Ramulu et al. [13] investigated the drilling properties of Al 6061 reinforced with $Al_2O_3$ MMCs using different drills. They reported that polycrystalline diamond (PCD) drills outperformed all other drills in terms of machined hole quality and drilling forces. Tosun and Muratoglu [14] studied the surface quality of drilled Al/SiC MMCs under dry cutting conditions. Other studies have stated that carbide drills provide less surface roughness compared with the high-speed steel (HSS) and TiN-coated HSS drills. Basavarajappa et al. [15] discussed the influence of machining parameters on the drilling properties of hybrid MMCs. They concluded that the cutting speed and feed rate were the most important machining parameters with respect to surface roughness and feed force. Ahamed et al. [16] investigated the drilling of Al–5% SiCp–5% $B_4$Cp hybrid composite with HSS tools and observed that the surface finish was improved under lower cutting speeds. Rajmohan et al. [17] reported that the surface roughness improved with increasing spindle speed and worsened with higher feed rates in the drilling of hybrid MMCs. Taşkesen and Kütükde [18,19] have studied the drilling behavior of $B_4C$-reinforced MMCs using HSS, TiAlN-coated carbide, and uncoated carbide drills under dry machining conditions. Their experimental results indicated that the thrust force increased with the reinforcement content and that surface quality reduced with increasing $B_4C$ content in the matrix. These studies also reported that the best surface roughness values were obtained when using TiAlN-coated carbide tools and that minimal cutting temperatures were measured at lower machining speeds and particle fractions together with relatively higher feed rates.

The main objective of this study is to investigate the behavior of $Al_2O_3$, $B_4C$, and SiC reinforcement particles on the mechanical and drilling properties of AA7039 composites. For this purpose, AA7039 and three AA7039 MMCs containing $Al_2O_3$, $B_4C$, and SiC reinforcement particles were manufactured by a powder metallurgy and hot-extrusion method. The hardness, bending strength, and elongation of specimens were studied and compared from the viewpoints of fracture surfaces and microstructures using scanning electron microscopy (SEM). Drilling experiments were performed to determine the effect of reinforcement elements on the machining of composites. The quality of machined surfaces is an important demand that increases manufacturing costs. The surface quality of a workpiece affects the durability and mechanical properties of the workpiece, including its creep, abrasion, corrosion resistance as well as its fatigue strength. Machining parameters and microstructural properties of composite specimens, which depend on their production method, are also important factors to consider for achieving a high-quality machined surface at minimal cost. Therefore, we investigated how the $Al_2O_3$, $B_4C$, and SiC particle reinforcements in AA7039-based composite materials affect the surface roughness for different drilling parameters under dry machining conditions. The surface roughness and chip formation were analyzed after drilling tests using a coated carbide drill under dry machining conditions. Furthermore, the experimental results were evaluated using analysis of variance (ANOVA), and the optimal drilling parameters were determined.

## 2. Experimental procedure

### 2.1. Production method of composite specimens

Three different AA7039 composite materials reinforced with 10 wt.% $Al_2O_3$, 10 wt.% $B_4C$, and 10 wt.% SiC were produced by a powder metallurgy and hot-extrusion method. The median particle size of the $Al_2O_3$, $B_4C$, and SiC powders was 7.1, 3.1 and 4.8 μm, respectively. For fabricating the experimental metal matrix composites, AA7039 and reinforcement powders were weighed on a Sartorius weighing instrument with $10^{-5}$ g precision and then separately mixed with 10% weight fractions of $B_4C$, SiC, and $Al_2O_3$ powders. The prepared compositions were uniformly blended one-by-one for 60 min in a three-dimensional Turbula mixer to obtain a homogenous mixture. The blended AA7039/$Al_2O_3$, AA7039/SiC, and AA7039/$B_4C$ compositions were cold-compacted at 300 MPa. The compacted specimens were sintered at 550 °C for 1 h to reduce the porosity and enhance the mechanical properties of composite materials. In the next step, the specimens were pre-heated to 500 °C for 1 h and then extruded using a hydraulic extrusion mold. Thus, AA7039-based MMC sheets were fabricated with dimensions of 285 × 24 × 86 $mm^3$. The sheets were solution heat-treated at 470 °C for 2 h to enhance the physical characteristics of the composite materials; the specimens were then hardened by quenching in water at room temperature to impart them with special mechanical properties. After the heat-treatment and quenching processes, the experimental specimens were aged at 120 °C for 2 h in a furnace.

### 2.2. Microstructural and mechanical analysis

The specimens were prepared by metallographic methods for testing of the hardness, the transverse rupture strength (TRS), and the particle size distribution of the reinforcement elements in the composites. SEM (JEOL JSM-6060LV) was used to investigate the microstructures, chemical compositions, and the fracture surfaces of the specimens. The hardness tests were performed using a Vickers hardness measurement machine (EMCO-TEST DuraVision 200) under a 3 kg load applied for a period of 5 s. Hardness measurements were performed at different regions, and the average value of hardness was calculated for each composite material. Five bending samples for each base alloy and composite material were cut into specimens with dimension of $25.4 \times 12.7 \times 6.35\ mm^3$ using wire electrical discharge machining (WEDM) according to Metal Powder Industries Federation Standard Test Methods for Metal Powders and Powder Metallurgy Products (MPFI-41, 1998). The TRS tests were performed using the Instron model 3369 universal testing machine. Fig. 1(b) shows the experimental setup for TRS. The mean value of bending strength was computed by testing four different specimens to determine the flexural stress of each composite material. The bending strength equation is given as

$$\sigma \equiv M \times y / I$$

$$y \equiv t/2$$

$$I \equiv w \times t^3 \Big/ 12$$

where $\sigma$ is stress, $M$ is the bending moment, $I$ is the moment of inertia, $w$ is the width of the specimen, $t$ is the thickness of the specimen, and $y$ is the distance from the axis. The maximum bending surface stress was taken as the stress at the midpoint of the samples [8] (Table 1).

### 2.3. Experimental design for drilling

Experimental studies were conducted according to the Taguchi method, which is a useful approach for reducing the experiment time and costs by minimizing the number of trials. Furthermore, it provides an easy, effective, and systematic approach to determining the ideal machining factors during experiments and minimizes the effects of uncontrolled factors. To study the influence of drilling parameters on the quality of machined surfaces, we conducted experiments using Taguchi's orthogonal array design of experiment, $L_{16}(4^3)$. In this experimental work, four different composite materials were machined under dry cutting environments and two drilling parameters (spindle speed and feed rate) were used as the drilling parameters with four levels. Table 2 shows the machining parameters for surface roughness and the four Taguchi experimental levels.

### 2.4. Machining process and drilling parameters

The drilling behavior of the specimens was studied on a Spinner VC750 vertical machining center with a maximum spindle speed of 12,000 rpm. The experimental setup of the drilling process is depicted in Fig. 1(a). A drill diameter of 8 mm and a hole length of 10 mm were chosen on the basis of previous study recommendations [18]. The spindle speed and feed rates were the drilling parameters for the experimental investigation. The experiments were conducted under dry machining environments. The machining parameters were selected according to the recommendation of the cutting tool manufacturer and preliminary tests results. The selected drilling parameters and experimental levels are presented in Table 2. A standard SK 40 tool holder with a single GC34-grade TiAlN-coated tool was used for the experiments. The drilling tool with an ISO designation of 460.1-0800-024A-M GC34 was produced by Sandvik; this tool is recommended for the drilling of multiple materials under different machining conditions.

**Table 1**
Chemical composition of AA7039.

| Chemical composition (wt.%) | | | | | | | | |
|---|---|---|---|---|---|---|---|---|
| Al | Mg | Zn | Cu | Si | Mn | Ti | Fe | Cr |
| 89.91 | 4.17 | 4.39 | 0.53 | 0.45 | 0.2 | 0.19 | 0.12 | 0.02 |

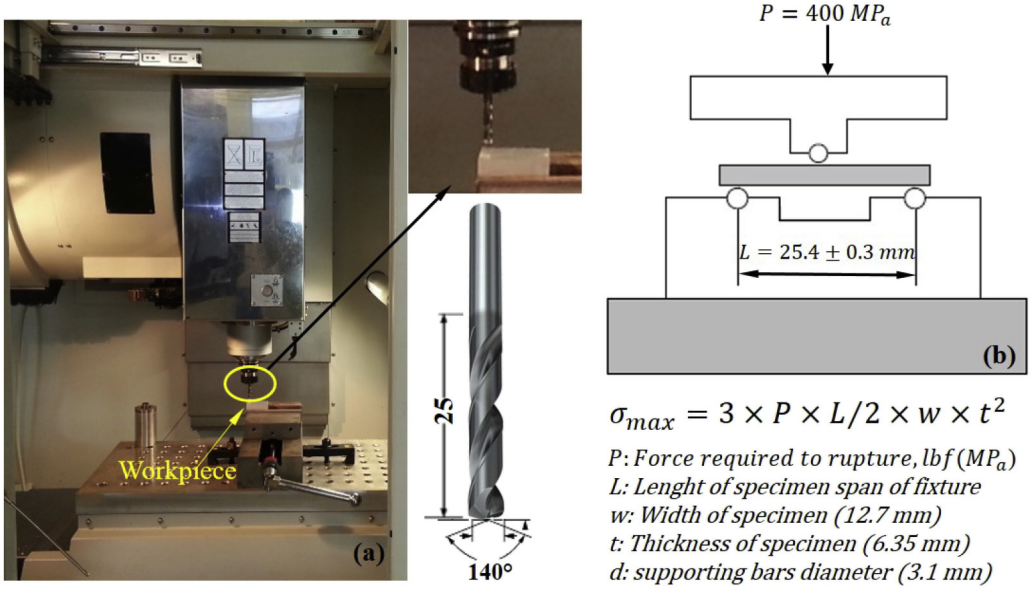


**Fig. 1.** Setup for drilling experiment (a) and the transverse rupture strength apparatus (b) [20].

**Table 2**
The machining parameters for surface roughness and the Taguchi $L_{16}(4^3)$ experimental levels.

| Factor | Notation | Unit | Level 1 | Level 2 | Level 3 | Level 4 |
|---|---|---|---|---|---|---|
| A – Material | *M* | pieces | AA7039 | 10 wt.% $Al_2O_3$ | 10 wt.% $B_4C$ | 10 wt.% SiC |
| B – Spindle speed | *S* | rev/min | 2000 | 2600 | 3400 | 4400 |
| C – Feed rate | $f_z$ | mm/tooth | 0.12 | 0.15 | 0.20 | 0.26 |
| Drill diameter | *d* | mm | 8 | 8 | 8 | 8 |
| Hole length | | mm | 10 | 10 | 10 | 10 |
| Workpiece dimension | | $mm^3$ | 40 × 40 × 10 | | | |

### 2.5. Surface roughness measurements

A hole was drilled into each sample using a new drilling tool, and measurements of the surface roughness of the drilled specimens were performed at six different areas using a Mitutoyo Surftest SJ-210 portable surface roughness measurement instrument (cut of length 0.25 mm). The surface roughness was measured according to standard ISO 1997. The minimum and maximum values for surface roughness were omitted from the measurement table, and the average roughness value for each composite material was determined by calculating the four remaining results.

## 3. Results and discussion

### 3.1. Microstructural and mechanical properties

AA7039-based MMCs reinforced with 10 wt.% $Al_2O_3$, 10 wt.% $B_4C$, and 10 wt.% SiC were produced by a powder metallurgy and hot-extrusion method. The composite specimens were subjected to hot-extrusion at 550 °C for 1 h in order to reduce the porosity and to obtain a uniform particle distribution within aluminum matrix. The microstructure, hardness, bending strength, and fracture surface of the composite materials were analyzed. SEM images of the microstructures of the composited reinforced with 10 wt.% $Al_2O_3$, 10 wt.% $B_4C$, and 10 wt.% SiC are depicted in Figs. 2–4, respectively. The reinforcement particles are commonly observed to be distributed uniformly within the composite structure as a consequence of the hot-extrusion production method and the three-dimensional mixing system. As shown in Fig. 2, better particle distribution was achieved in $Al_2O_3$ particle reinforced composite specimen with 7.1 μm particle size. On the other hand, the particle distribution of $B_4C$ with 3.1 μm particle size and SiC with 4.8 μm particle size was not adequately uniform. Some dispersed heterogeneous particles were observed to be agglomerated under high magnification [22]. Figs. 3 and 4 show the SEM images of the 10 wt.% $B_4C$ and 10 wt.% SiC particle-reinforced composites in which particle clustering are clearly shown. This can be related to the particle size of the reinforcement elements in the composites. Kok [23] concluded that the dispersion of the coarser $Al_2O_3$ particles was uniformly distributed while the finer particles caused the agglomeration and porosity in the aluminum matrix. We have observed some interfacial voids around the reinforcement particles as depicted in Figs. 2–4. These interfacial voids are the result of the mainly wetting characteristic of the matrix and reinforcement particles $Al_2O_3$, $B_4C$ and SiC. Fig. 2 shows a better interfacial bonding effect between the $Al_2O_3$ particles and aluminum alloy as compared to the other two composite specimens. Although, it was observed that some voids form only at one side of the $Al_2O_3$ particles and matrix interface, the better particle–matrix bonding was achieved in the fracture analysis as shown in Fig. 6. In the composite specimen of AA7039 reinforced with $B_4C$ and SiC, the voids are evident around the particles in the matrix indicating a poor bonding [19]. As depicted in Figs. 5–9, the mechanical and machinability properties of these composites are directly related to the uniformly distribution of the particles and bonding at the reinforcement/matrix interfaces.

The mechanical properties of the specimens, such as their hardness, transverse rupture strength, and elongation, were evaluated. Fig. 5 shows the influence of the reinforcement elements on the mechanical properties of the composite specimens and AA7039. Ibrahim et al. [6] revealed that the hardness of the composites was changed as a function of the aging temperatures. Higher hardness values were obtained for aging temperatures up to 200 °C and the hardness of base aluminum alloy was significantly improved from ~20 BHN up to ~70 BHN. Baradeswaran and Perumal [8] concluded that increasing the content of $Al_2O_3$ ceramic particles results in remarkable increase in the hardness and elongation of Al 7075/$Al_2O_3$/graphite hybrid composites. The higher hardness value was obtained in the hybrid composites containing 8 wt.% $Al_2O_3$ ceramic particles. In another study, they [21] noticed that the hardness and flexural strength of Al 7075–$B_4C$ composites was increased with the addition of the $B_4C$ particles. We concluded that the mechanical properties were affected by the reinforcement particles used in the composite structure. The composite material composed of AA7039 reinforced with 10 wt.% $Al_2O_3$ exhibited the highest hardness and TRS values among the investigated materials. The bending strength of the 10-wt.%-$Al_2O_3$-reinforced composite material was better than that of the other composite specimens and that of the unreinforced AA7039 matrix alloy. These findings are in good agreement with the result of the previous researchers [8,10]. The elongation of the composite materials upon the addition SiC, $B_4C$, and $Al_2O_3$ particles was reduced by a decrease in ductility compared with that of the pure AA7039. However, the greatest elongation among the investigated composite materials was achieved with AA7039/$Al_2O_3$. The elongation of the specimens depicted in Fig. 5(c) is in good agreement with that reported by Baradeswaran et al. [8] and Ibrahim et al. [6]. The increased TRS, elongation, and hardness of the Al7039/$Al_2O_3$ composite material compared with those of the pure AA7039 and the other investigated composite specimens are due to the good interface bonding effect of $Al_2O_3$ particles in the matrix structure. Lower TRS, elongation, and hardness values were observed in the case of AA7039 reinforced with SiC particles. Similar results were reported from Doel and Bowen [9] for the Al 7075 alloy reinforced with SiC ceramic particles. The decreasing mechanical properties of $B_4C$ and SiC reinforced composites may be a consequence of agglomeration and weak bonding at the particles/matrix interface. In addition to this, the specimens for bending and hardness tests were prepared using WEDM, and the hardness measurements of the composite specimens were performed after the WEDM process. Therefore, during the WEDM operation, SiC and $B_4C$ particles may have partially separated from the matrix because of their weak interfacial bond, leaving behind small holes and cavities. These defects could lead to a decrease in the hardness of the $B_4C$- and SiC-reinforced composite materials [24].

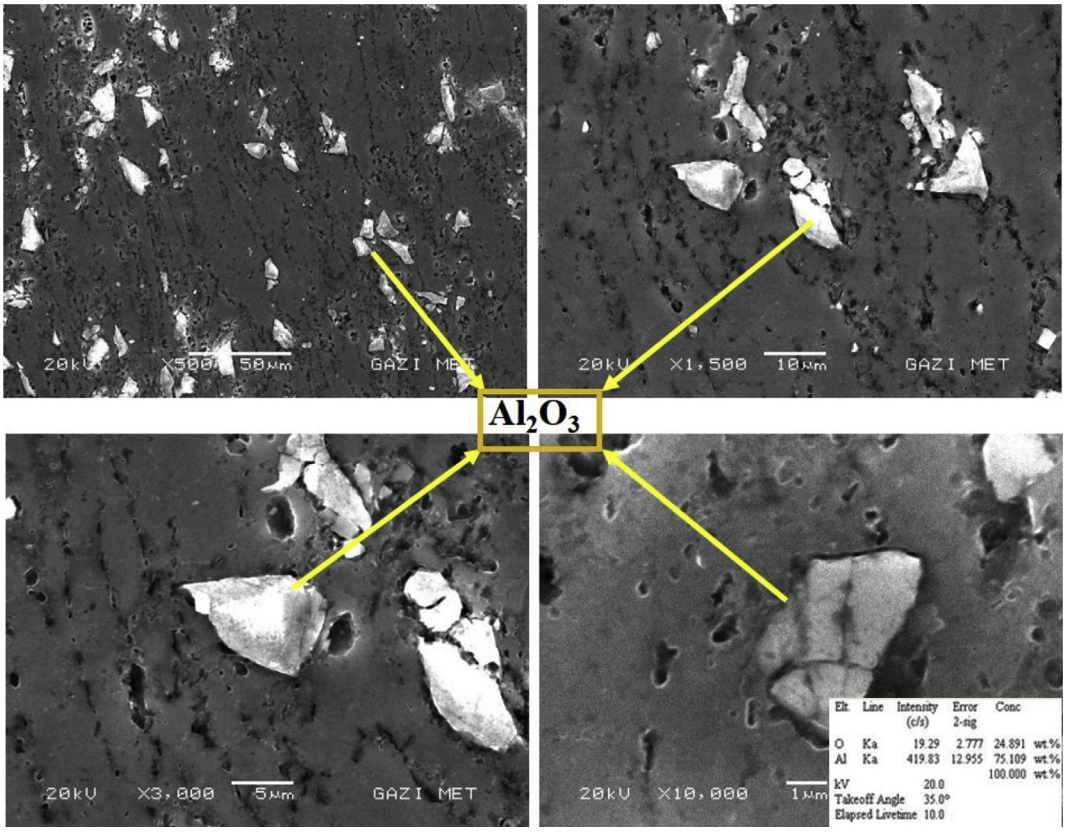


**Fig. 2.** SEM micrographs showing the distributions and interfaces of $Al_2O_3$ particles.

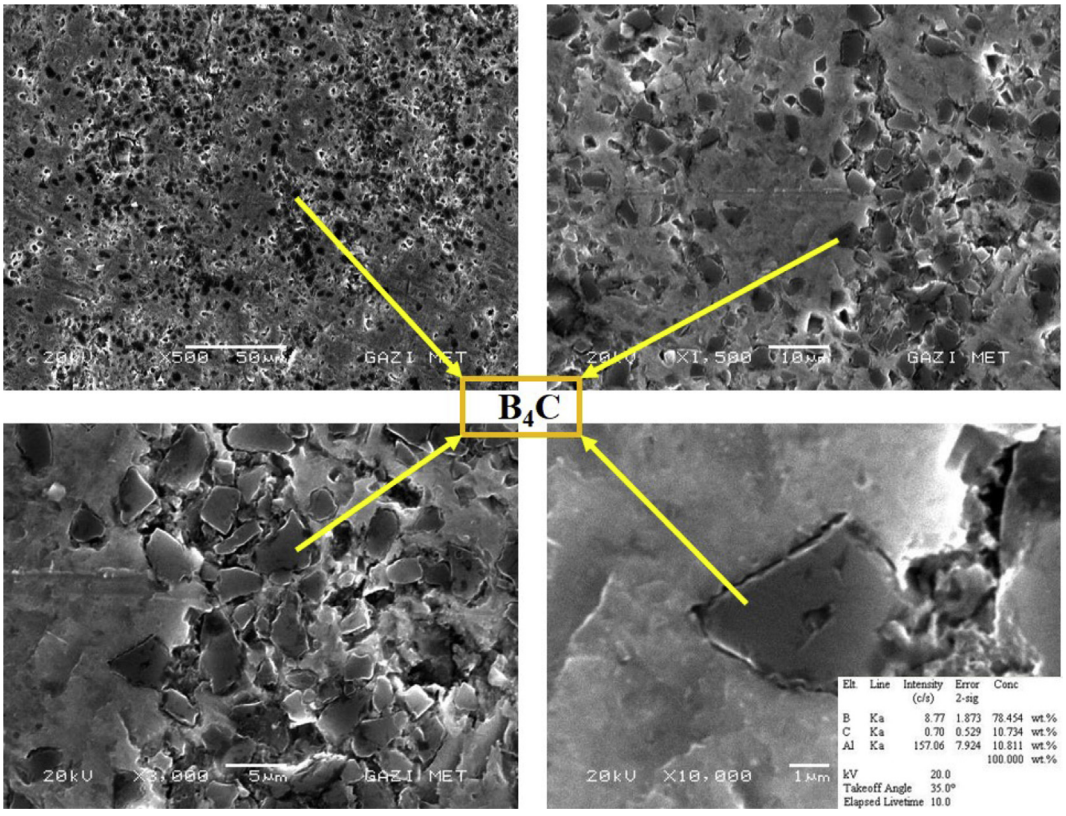


**Fig. 3.** SEM micrographs of machined AA7039/$B_4C$ composite materials.

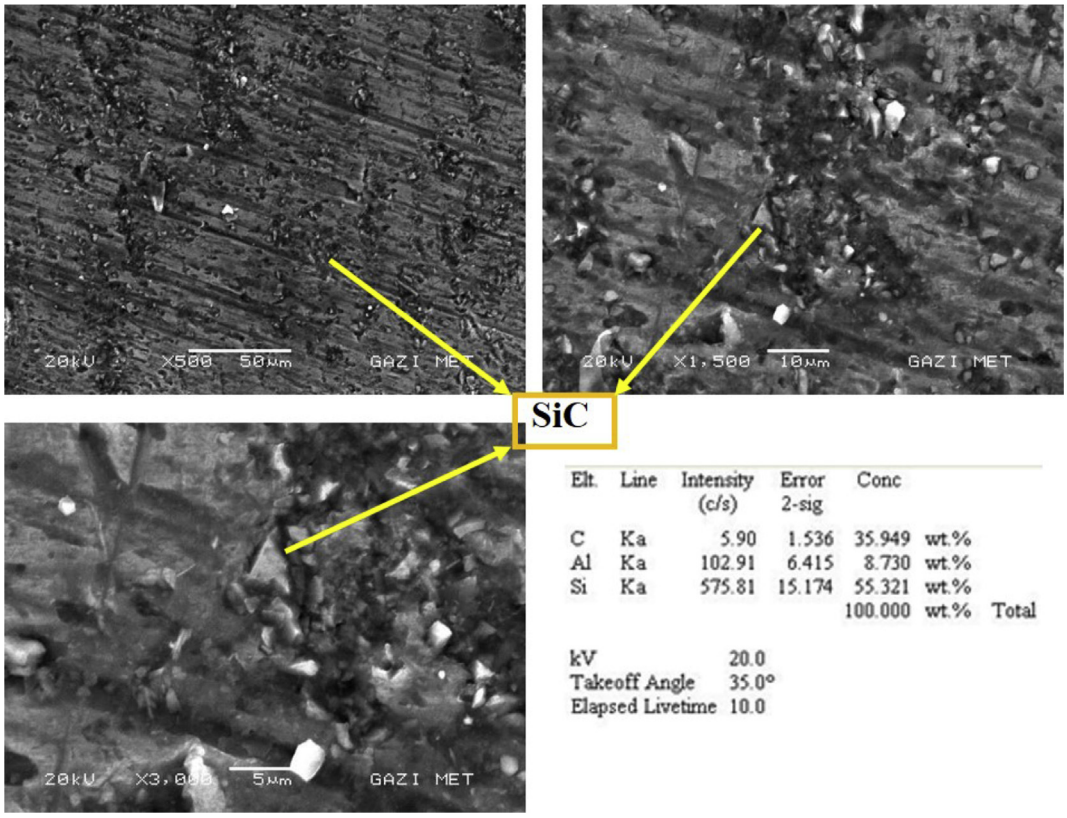


**Fig. 4.** SEM micrographs of machined AA7039/SiC composite materials.

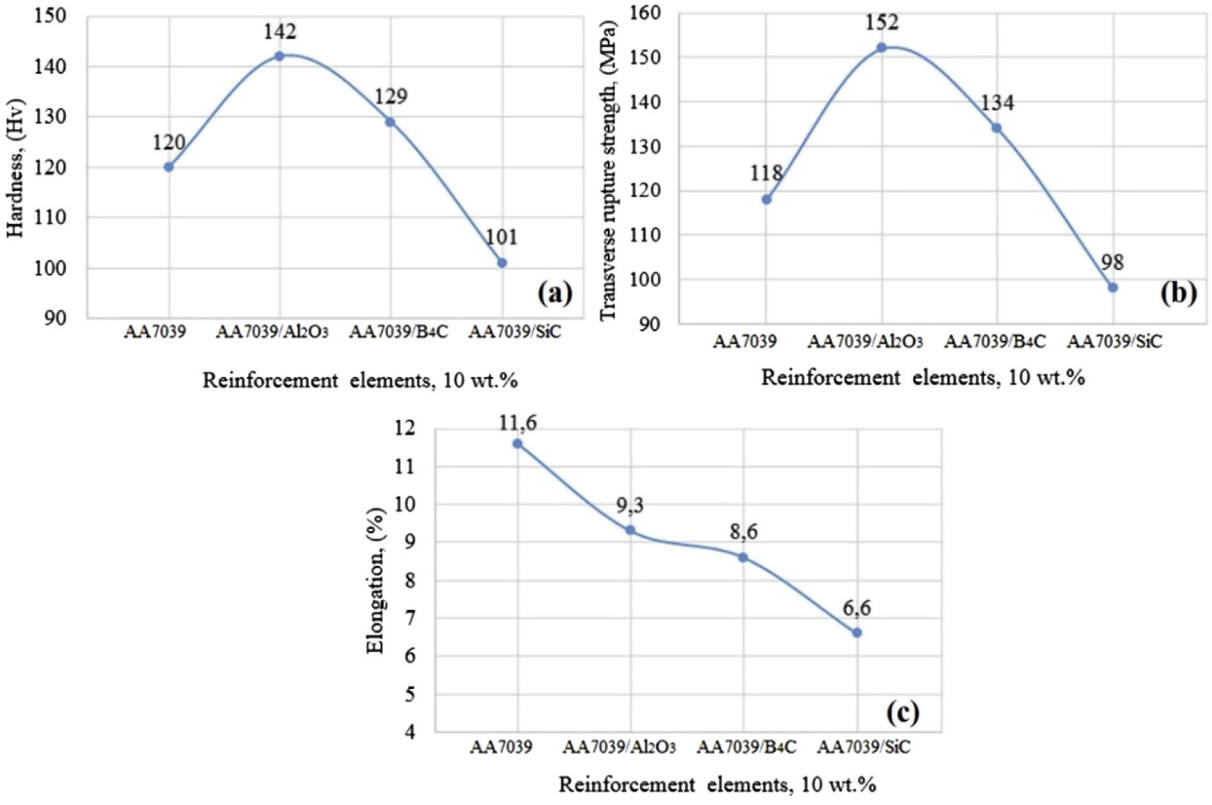


**Fig. 5.** Hardness (a), transverse rupture strength (b), and elongation (c) of the composite materials under study.

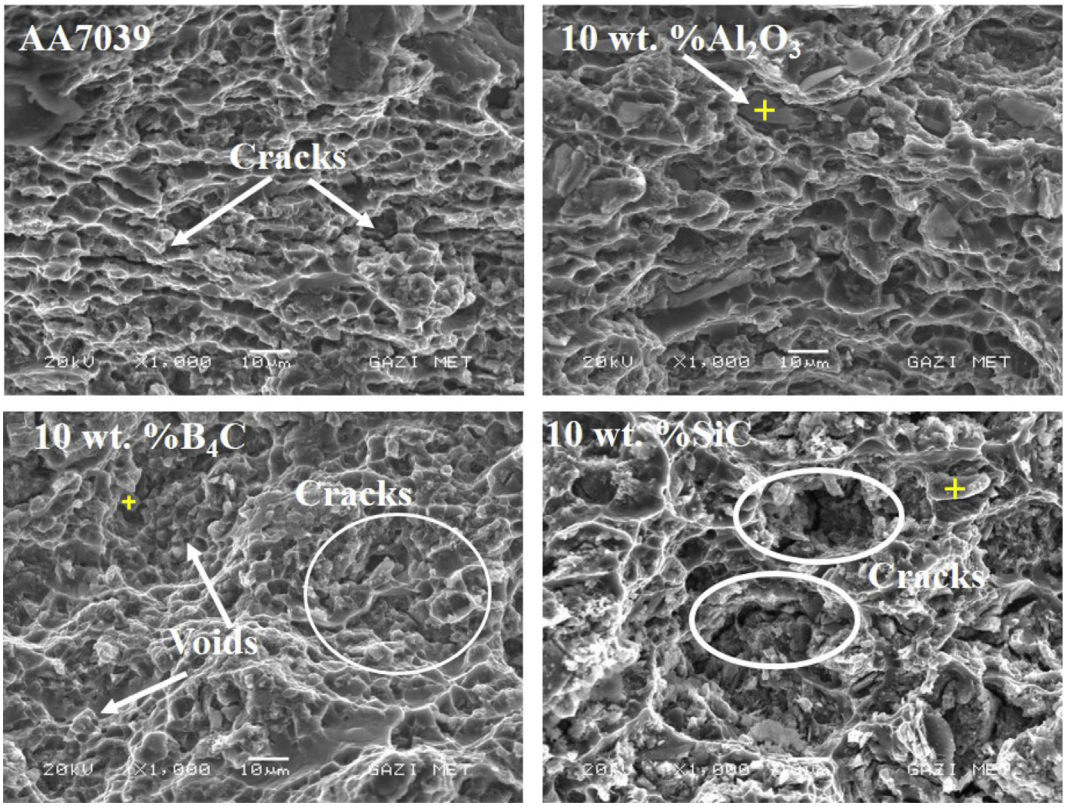


**Fig. 6.** SEM fractographs for fracture surfaces of AA7039, AA7039/$Al_2O_3$, AA7039/$B_4C$, and AA7039/SiC.

### 3.2. Fractography

Three AA7039-based composites with the same volume fraction of reinforcement elements were subjected to TRS tests to investigate the fracture surfaces and interfacial bonding behaviors between the aluminum matrix and the reinforcement particles. The fracture surfaces of the AA7039 and composite specimens were evaluated by SEM to investigate their fracture surface morphology. SEM fractographs of the fracture surfaces of these composite specimens and AA7039 are presented in Fig. 6. All the specimens exhibited ductile fracture behavior with many fine dimples at fractured surfaces. Microcracks were observed in the fracture surfaces of the AA7039, AA7039/$B_4C$, and AA7039/SiC specimens at the matrix interfaces and progressed through the reinforcement particles. However, no cracks or voids and clear contours were observed in the fracture surface of the AA7039/$Al_2O_3$ composite specimen around the interfaces of the matrix and the $Al_2O_3$ particles. This result indicates that the composite specimen reinforced with $Al_2O_3$ exhibited sufficient ductility for achieving greater flexural strength. The $Al_2O_3$ particles prevented the quick propagation of cracks and limited the deformation of the composite, which resulted in enhanced bending strength of the specimens. The $Al_2O_3$ particles are uniformly distributed in the matrix structure and are well adhered to the aluminum matrix. As evident in Fig. 6, $Al_2O_3$ particles exhibit good bonding and are not separated from the fractured surfaces. Among the three AA7039-based composite materials, the AA7039/$Al_2O_3$ specimen exhibited the strongest interfacial bonding between the matrix and the reinforcement particles.

Ductile fracture was observed in the fractured surfaces of AA7039/B4C and AA7039/SiC as a consequence of the microvoid formation mechanism. Crack propagation was observed throughout the matrix, and fine ductile dimples were evident at the fracture surfaces of the composite specimen reinforced with $B_4C$ and that reinforced with SiC [7]. The weakest bonding structure was observed in the fracture surface of AA7039/$B_4C$ because the conglomeration of particles decreased the ductility and because the adherence of the aluminum matrix alloy was weak. Voids and dimples were created at the interfaces of the reinforcement particles and the aluminum matrix, thereby indicating weak bonding. In the AA7039/SiC matrix structure, interfacial bonding appears to be stronger than that in the AA7039 reinforced with $B_4C$ particles. SiC particles were detached from the AA matrix at the fracture surface of the composite because they were well bonded with the matrix structure. Hence, these broken SiC particles left large voids and gaps, resulting in larger microcracks compared with those in the composite containing $B_4C$ particles.

### 3.3. Drilling properties

The drilling parameters were designated using Taguchi techniques. The surface roughness of the drilled specimens was measured at six different areas; the minimum and maximum results for surface roughness were eliminated and the mean surface roughness was calculated using the four remaining values. The average roughness values for each specimen are presented in Table 3. The effect of noise in the experimental system is minimized by maximization of the $S/N$ ratio; hence, the optimal machining parameters were determined on the basis of the highest $S/N$ for the cutting parameters. The optimal drilling parameters and the results obtained for each set of drilling parameters are given in Table 4. The mean effect of drilling parameters on surface roughness is shown in Fig. 7. From the experimental findings, it was observed that the surface quality was affected from the type of reinforcement

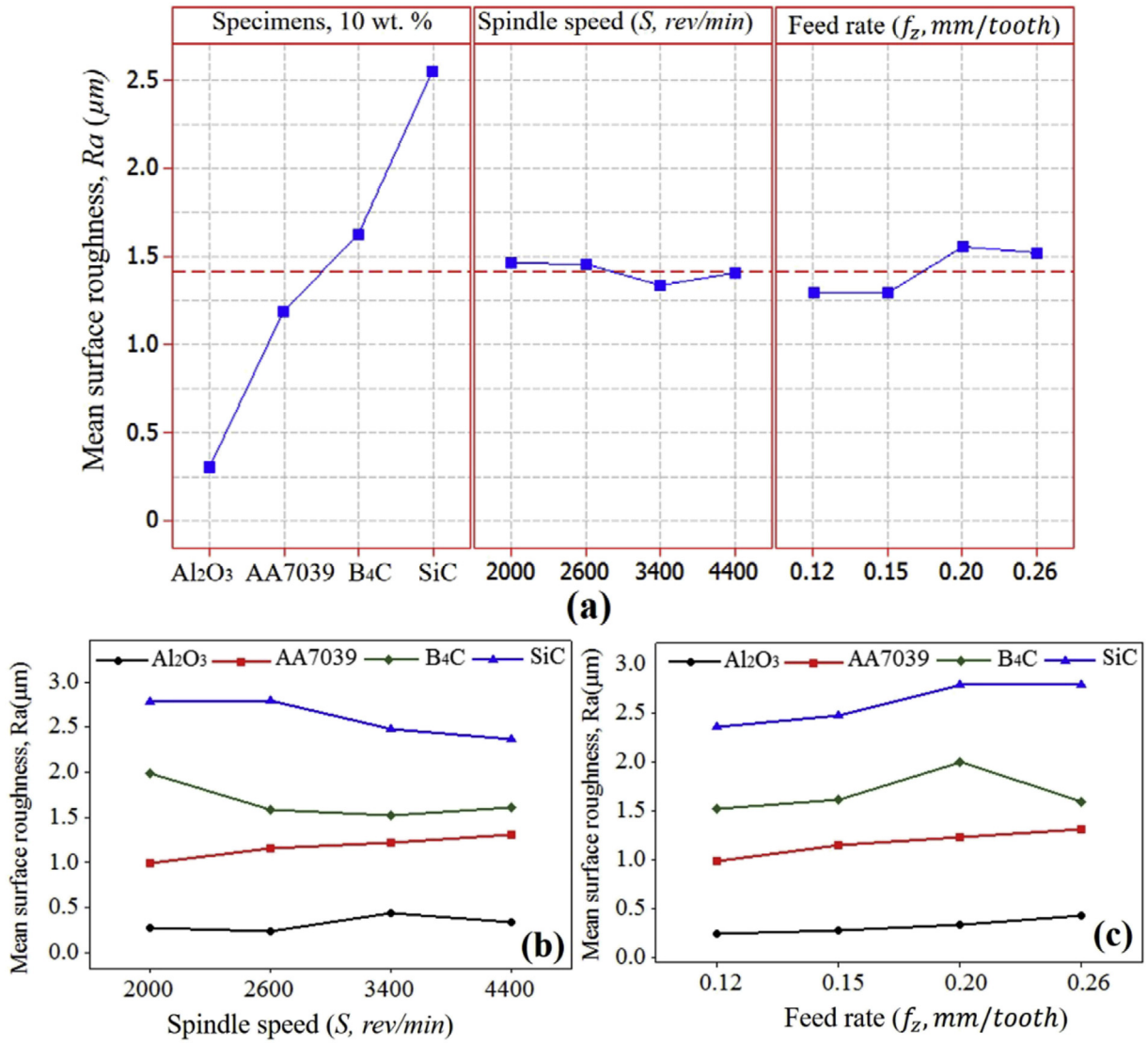


**Fig. 7.** The mean effects of drilling parameters (a), interaction effect of spindle speed and material (b), interaction effect of feed rate and material (c) on hole surface roughness.

elements in matrix structure. Surface roughness results were remarkably improved in the drilling 10 wt.% $Al_2O_3$ composites compared with the aluminum alloy and other two composite specimens in all experimental trials [figures (a), (b) and (c)]. As can be seen from the figures, the average surface roughness values were increased with increasing feed rates in drilling of all composite specimens. The increase in the spindle speeds does not have not a meaningful effect on the machined surface roughness of the composites (Table 5).

The optimal drilling parameters were determined according to the response surface table for *S*/*N* ratios in Table 4. The best hole surface roughness was obtained with AA7039 reinforced with 10 wt.% $Al_2O_3$ ($A_1$), a spindle speed ($B_2$) of 2600 rpm, and a feed rate ($C_1$) of 0.12 mm/tooth. ANOVA was performed to statistically analyze the experimental results for surface roughness. On the basis of the ANOVA results, the reinforcement element in the composite structure is the parameter that most strongly influences the surface roughness. The interaction effects of spindle speed and feed rate for all experimental specimen have not shown a statistical significance on surface roughness when analyzed together with all experimental specimens. The machined surface of the materials was significantly affected from the type of the reinforcement particles and their dispersion in the matrix structure. The lowest surface roughness values are achieved in the drilling of the AA7039/$Al_2O_3$ among the experimental specimens. The highest surface roughness values are measured in a wide range from the 0.99 μm to 2.80 μm in the drilling of aluminum alloy and the other two composite specimens. Thus, the most effective factor on surface roughness was the type of material with percentage contributions of 97% according to the ANOVA results.

Excellent surface quality was achieved in the drilling of the AA7039/$Al_2O_3$ composite specimen, and the surface roughness values ranged from 0.23 μm to 0.43 μm. In contrast, the drilled AA7039, AA7039/$B_4C$, and AA7039/SiC specimens exhibited lower finished surface quality. The worst surface roughness values were measured in the case of drilled AA7039/SiC composite specimens. Similar results related to the milling of AA7039 and an AA7039/$Al_2O_3$ composite specimen have been previously reported [5]. Fig. 8 shows the relationship between the spindle speed and feed rate on surface roughness when the experimental materials were examined individually. Better surface roughness values were measured for specimens drilled using lower feed rates; increasing feed rates resulted in decreased finished surface quality in the drilling of all specimens. This result is expected because more chips are removed

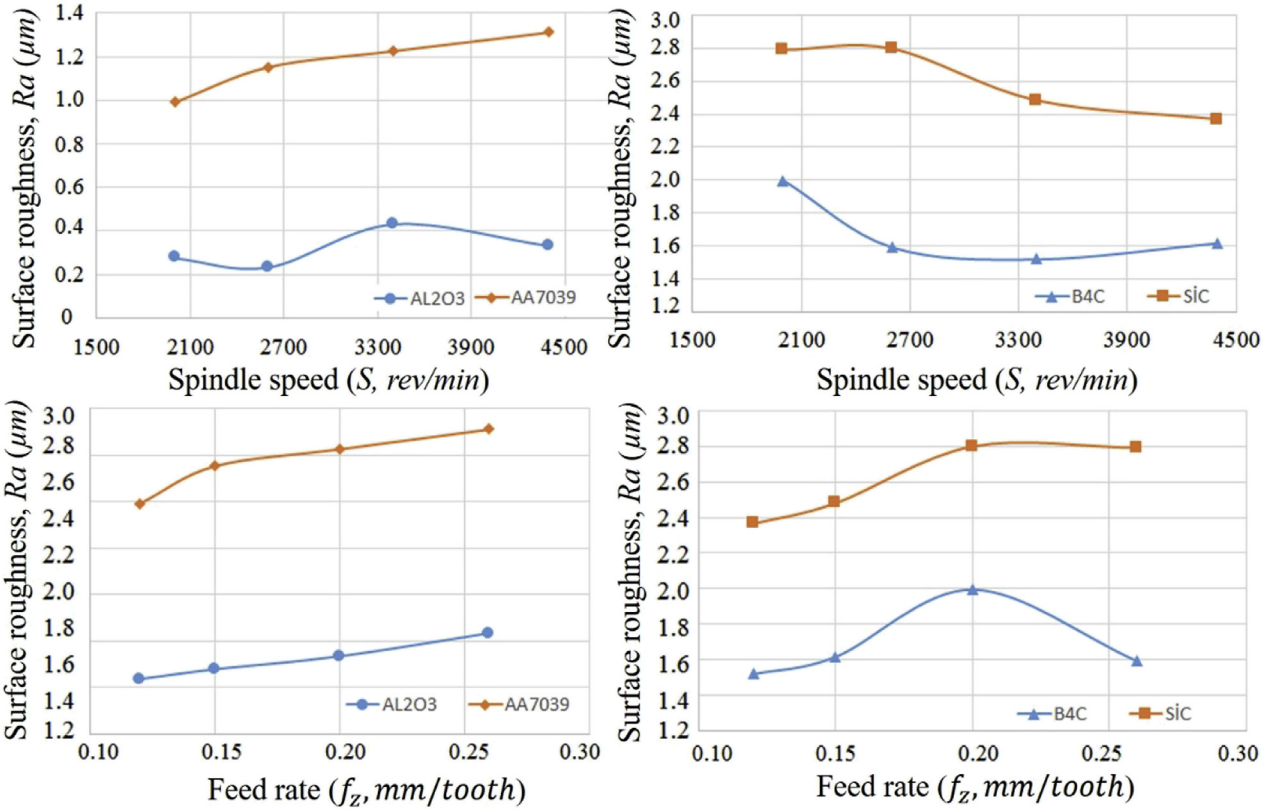


**Fig. 8.** Effect of spindle speed and feed rate on surface roughness in the drilling of specimens.

from workpiece at higher feed rates and drilling tool interface subjected to more friction and interruption. Surface quality was improved at higher spindle speed due to decreasing the coefficient of friction between the drilling tool and workpiece in the drilling of composite specimens. However, surface roughness values are increased at higher spindle speed in the machining of aluminum 7039 alloy (Fig. 8). This may be attributed to the built up-edge (BUE) formation. It is evident that the flow of material was observed on the machined surface of AA7039 in Fig. 9(a).

To elucidate the effect of reinforcement elements and the drilling parameters on the hole surface, we cut the drilled specimens into two equal pieces and examined the machined surfaces of the holes using SEM. Figs. 9 and 10 show SEM micrographs of the drilled surfaces of the specimens. Examination of the machined surfaces leads to the conclusion that higher feed rates result in heavy surface damage in the AA7039 matrix alloy and composite specimens because of the higher cutting temperature and greater contact pressure [25]. An increase in cutting temperature at the tool–workpiece surface increases the softening of the aluminum matrix during the machining process and leads to plastic deformation of the specimens. The SEM micrograph of AA7039 matrix alloy in Fig. 9(a) reveals the flow of material along the drilling direction, which is mainly characterized by plastic deformation. The softened aluminum is transferred from the workpiece to the drilling-tool surface. This BUE formation on the cutting tool is caused by scratches on the hole surface during the drilling process because of attrition between the tool and workpiece. The generation of plastic deformation and BUE formation on the cutting surface of drill adversely affected the machined surface of AA7039. However, roughness values commensurate with a high-quality surface were achieved in the case of drilling of the composite specimen of AA7039 reinforced with a 10 wt.% $Al_2O_3$, as evident in Fig. 9(b).

As previously discussed, among the investigated reinforced specimens, the composite specimen reinforced with 10 wt.% $Al_2O_3$ particles exhibited the greatest interfacial bonding in the matrix structure. During the experiments, the $Al_2O_3$ particles strengthened the aluminum matrix by increasing its ductility and also supported the softer matrix. The lack of BUE creation on the cutting tool is also responsible for these improvements. As shown in Fig. 10(a) and (b), a heavy flow of material along the drilling direction is evident on the finished hole surface of the composite specimens reinforced with 10 wt.% $B_4C$ and 10 wt.% SiC because of the increasing machining temperature. In the drilling of the composite reinforced with 10 wt.% $B_4C$, the $B_4C$ particles were partially or totally separated from the softening matrix because of the heterogenic structure of the composite. The separated particles resulted in large scratches, cavities, and grooves on the machined surface because they were dragged by the tool during the drilling process. In the case of the drilled SiC-reinforced composites, very poor quality of the finished surface was observed. This result is attributed to the wetting properties of SiC particles in the matrix structure. During machining, the hard SiC particles in the matrix adhered to the cutting tool, resulting in the formation of BUE, and contacted the drilled surface by serving as small cutting edges on the drilling tool [26]. The presence of crushed SiC particles, cavities, and grooves and the flow of material on the drilled surface are evident in Fig. 10(b). The presence of SiC particles in the matrix structure during the drilling process resulted in poor surface quality compared with that of the composites reinforced with other materials.

### 3.4. Chip formation

Fig. 11 shows SEM micrographs of chip shapes produced during the drilling of the AA7039 matrix alloy and composite specimens.

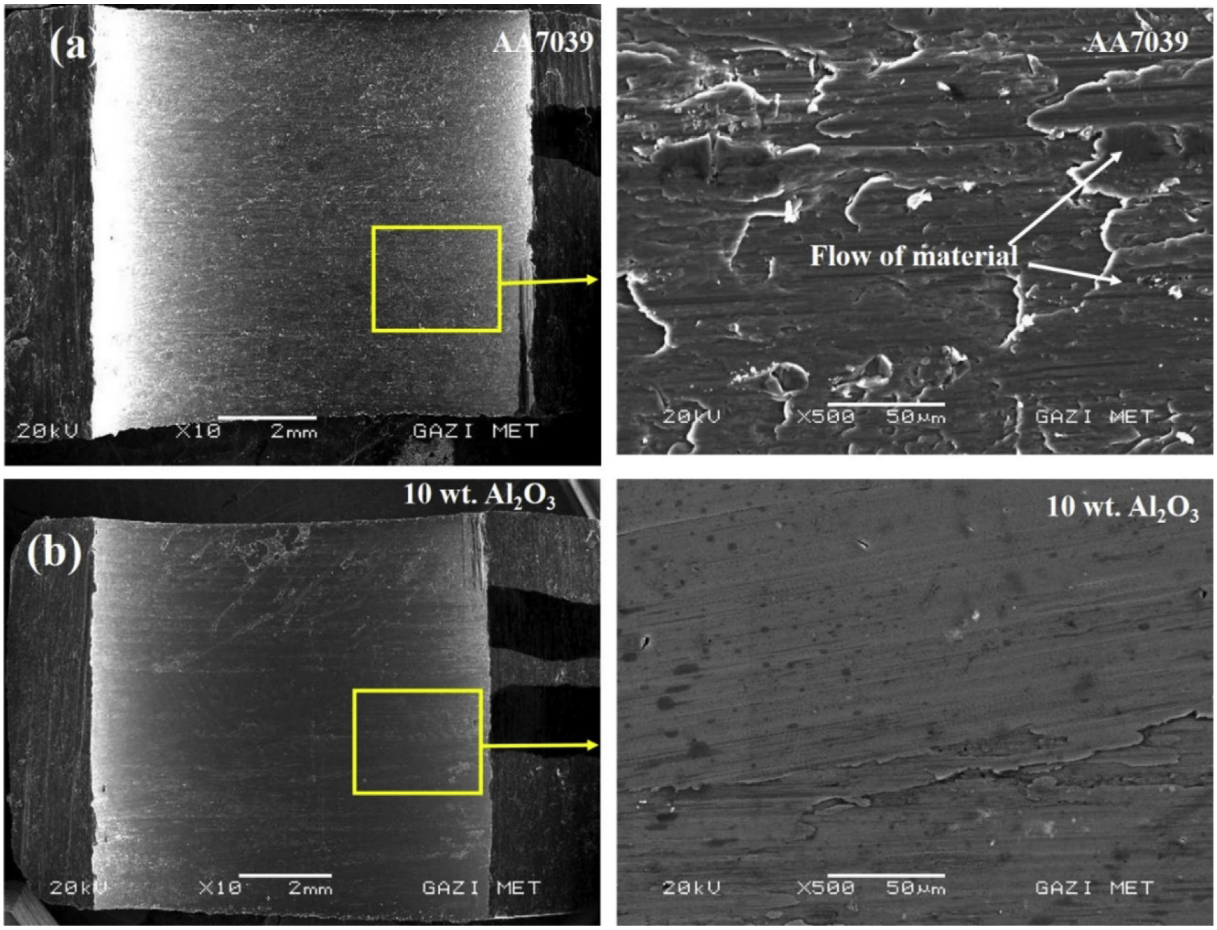


**Fig. 9.** SEM micrographs of drilled surfaces of (a) AA7039 ($S = 2000$ rev/min, $f_z = 0.12$ mm/tooth) and (b) AA7039/$Al_2O_3$ ($S = 2600$ rev/min, $f_z = 0.12$ mm/tooth).

Chip formation is affected by microstructure, ductility, and machining parameters such as cutting speed and feed rate. Figs. 10 and 11 indicated that the removed chip surfaces and the machined surface of the workpiece were exhibited the similar surface properties under the same drilling conditions. The chip forms are additional evidence related to the previously discussed microstructural properties, fractural surface analysis, and machined surface quality observed after the drilling process. During machining of the MMCs, chip deformations along the shear zone and stress concentrations occur because of the presence of hard particles. During this process, some particles are debonded from the matrix, thereby initiating the formation of cracks and some small voids. The composite specimens reinforced with harder particles exhibited good chip disposability and generated shorter

**Table 3**
The surface roughness measurement results and *S*/*N* ratio values for surface roughness.

| *N* | Control factors | | | Surface roughness results | | | | Average surface roughness, *Ra* (μm) | *S*/*N* ratio for *Ra* (dB) |
|---|---|---|---|---|---|---|---|---|---|
| | *A* | *B* | *C* | | | | | | |
| | Material (*M*) | Spindle speed (*S*) | Feed rate ($f_z$) | $Ra_1$ (μm) | $Ra_2$ (μm) | $Ra_3$ (μm) | $Ra_4$ (μm) | | |
| 1 | AA7039/$Al_2O_3$ | 2000 | 0.15 | 0.282 | 0.325 | 0.259 | 0.245 | 0.278 | 11.131 |
| 2 | AA7039/$Al_2O_3$ | 2600 | 0.12 | 0.184 | 0.203 | 0.226 | 0.331 | 0.236 | 12.557 |
| 3 | AA7039/$Al_2O_3$ | 3400 | 0.26 | 0.319 | 0.415 | 0.507 | 0.49 | 0.433 | 7.276 |
| 4 | AA7039/$Al_2O_3$ | 4400 | 0.20 | 0.293 | 0.369 | 0.341 | 0.334 | 0.334 | 9.535 |
| 5 | AA7039 | 2000 | 0.12 | 1.002 | 0.962 | 0.909 | 1.091 | 0.991 | 0.075 |
| 6 | AA7039 | 2600 | 0.15 | 1.186 | 1.142 | 1.102 | 1.183 | 1.153 | −1.236 |
| 7 | AA7039 | 3400 | 0.20 | 1.111 | 1.168 | 1.171 | 1.453 | 1.226 | −1.773 |
| 8 | AA7039 | 4400 | 0.26 | 1.308 | 1.282 | 1.316 | 1.342 | 1.312 | −2.361 |
| 9 | AA7039/$B_4C$ | 2000 | 0.20 | 2.125 | 2.178 | 2.086 | 2.401 | 2.198 | −6.01 |
| 10 | AA7039/$B_4C$ | 2600 | 0.26 | 1.624 | 1.602 | 1.552 | 1.598 | 1.594 | −4.048 |
| 11 | AA7039/$B_4C$ | 3400 | 0.12 | 1.508 | 1.618 | 1.478 | 1.48 | 1.521 | −3.643 |
| 12 | AA7039/$B_4C$ | 4400 | 0.15 | 1.594 | 1.548 | 1.566 | 1.768 | 1.619 | −4.183 |
| 13 | AA7039/SiC | 2000 | 0.26 | 2.252 | 3.186 | 2.994 | 2.731 | 2.791 | −8.916 |
| 14 | AA7039/SiC | 2600 | 0.20 | 2.243 | 3.458 | 2.596 | 2.898 | 2.799 | −8.941 |
| 15 | AA7039/SiC | 3400 | 0.15 | 2.336 | 2.584 | 2.234 | 2.774 | 2.482 | −7.896 |
| 16 | AA7039/SiC | 4400 | 0.12 | 2.382 | 2.266 | 2.549 | 2.266 | 2.366 | −7.482 |

**Table 4**
Response table for *S*/*N* ratios for surface roughness; smaller values are better.

| Level | Signal-to-noise ratios | | | Response table for means | | |
|---|---|---|---|---|---|---|
| | Material (*M*) | Spindle speed (*S*) | Feed rate ($f_z$) | Material (*M*) | Spindle speed (*S*) | Feed rate ($f_z$) |
| 1 | 10.1247 | −0.9301 | 0.37670 | 0.3199 | 1.5145 | 1.2786 |
| 2 | −1.3237 | −0.4171 | −0.5461 | 1.1708 | 1.4454 | 1.3828 |
| 3 | −4.4711 | −1.5089 | −1.7970 | 1.6828 | 1.4155 | 1.5892 |
| 4 | −8.3087 | −1.1226 | −2.0123 | 2.6097 | 1.4078 | 1.5325 |
| Delta | 18.4334 | 1.0918 | 2.3891 | 2.2898 | 0.1067 | 0.3106 |
| Rank | 1 | 3 | 2 | 1 | 3 | 2 |

**Table 5**
Analysis of variance for surface roughness.

| Source | DF | SeqSS | AdjMS | *F* | *P* | Contribution rate (%) |
|---|---|---|---|---|---|---|
| *M* | 3 | 757.316 | 252.439 | 250.30 | 0.000 | 97 |
| *S* | 3 | 2.474 | 0.825 | 0.82 | 0.530 | |
| $f_z$ | 3 | 15.046 | 5.015 | 4.97 | 0.046 | 2 |
| Error | 6 | 6.051 | 1.009 | | | 1 |
| Total | 15 | 780.888 | | | | 100 |

and low hardness increased the smeared material at the tool–chip interface, resulting in grooves at the inner surface of the chips.

The presence of hard $B_4C$ and SiC particles altered the plastic deformation characteristics of the aluminum matrix alloy. These reinforcement elements reduced the ductility and led to more fragment and more brittle chip formation, producing saw-toothed chips during drilling. Cracks, a heavy flow of metal, and flakes were observed on the chip surfaces of composite specimens rein-

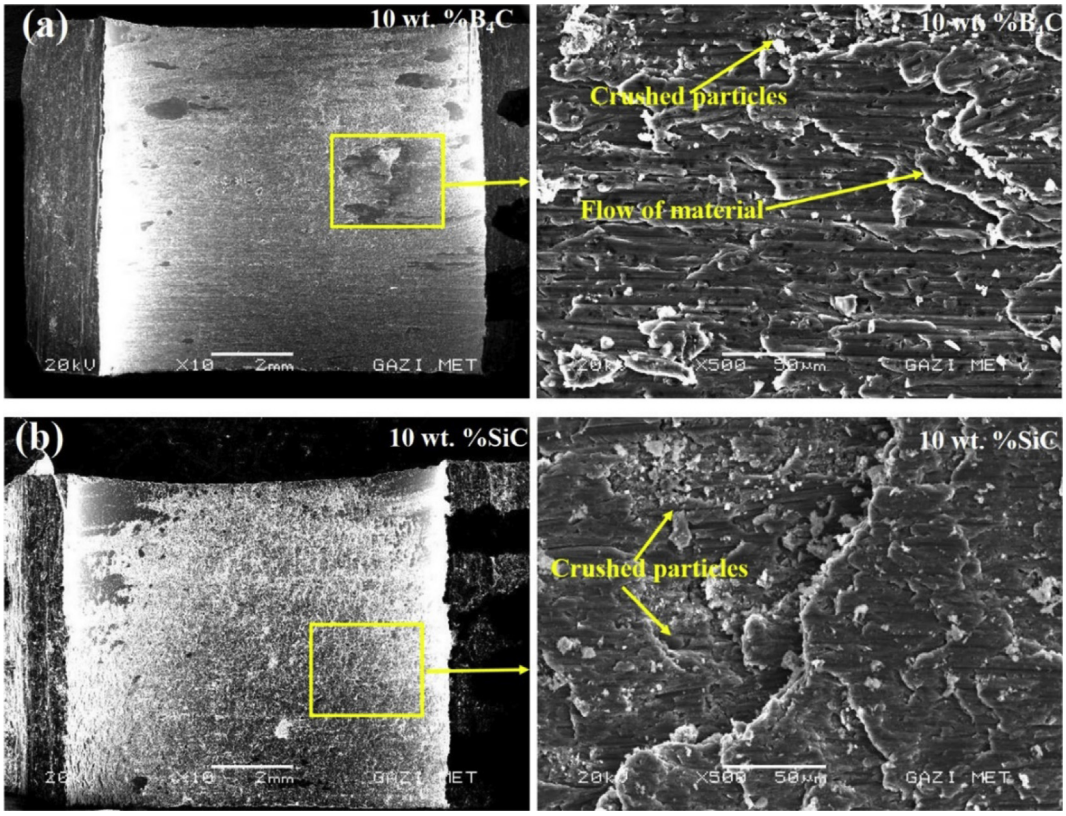


**Fig. 10.** SEM micrographs of drilled surfaces of (a) AA7039/$B_4C$ ($S$ = 3400 rev/min, $f_z$ = 0.12 mm/tooth) and (b) AA7039/SiC ($S$ = 4400 rev/min, $f_z$ = 0.12 mm/tooth).

chips. In contrast, the ductile aluminum matrix alloy produced longer chips with adhering material, which damaged the machined surface of the specimen [27–30]. Ductile machining with short chips was achieved in drilling AA7039/$Al_2O_3$ specimens without damage to the machined surface of the hole. The chips of the 10 wt.% $Al_2O_3$ composite specimen exhibited a smooth and shiny surface, with greater ductility than the aluminum matrix alloy. A small-quantity flow of material and narrow grooves along the cutting direction was observed on the surface of the AA7039 matrix alloy chip because of plastic deformation. These results are attributed to the high ductility of the matrix alloy. Hence, high ductility forced with $B_4C$ and SiC. The modification of the mechanical and microstructural properties by the particle reinforcement in the aluminum matrix changed the mechanism of chip formation to cracking; saw-toothed, segmented flakes; and interface debonding.

## 4. Conclusions

In this study, AA7039-based metal matrix composites reinforced with 10 wt.% $Al_2O_3$, 10 wt.% $B_4C$, and 10 wt.% SiC were successfully fabricated using a powder metallurgy and hot-extrusion method. The effects of $Al_2O_3$, $B_4C$, and SiC reinforcement particles on the

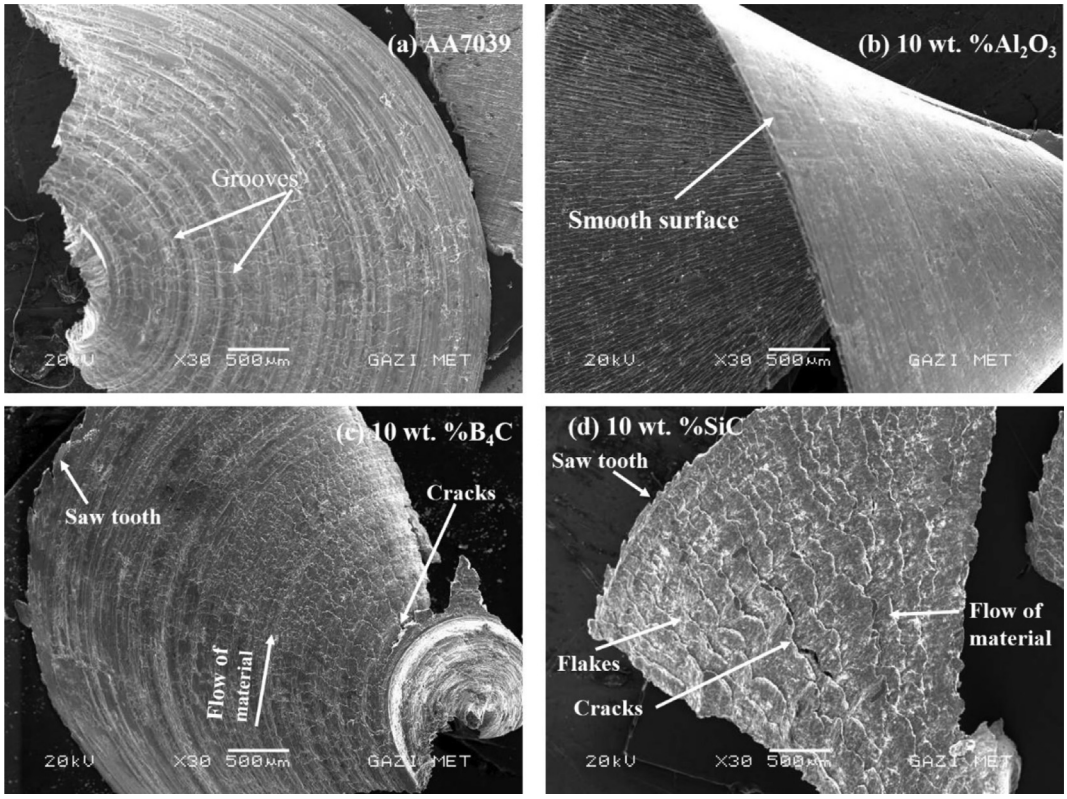


**Fig. 11.** SEM micrographs of the chips formed during the drilling of specimens. (a) AA7039 ($S$ = 2000 rev/min, $f_z$ = 0.12 mm/tooth), (b) AA7039/$Al_2O_3$ ($S$ = 2600 rev/min, $f_z$ = 0.12 mm/tooth), (c) AA7039/$B_4C$ ($S$ = 3400 rev/min, $f_z$ = 0.12 mm/tooth) and (d) AA7039/SiC ($S$ = 4400 rev/min, $f_z$ = 0.12 mm/tooth).

mechanical and drilling properties of AA7039 were investigated. The experimental findings are summarized as follows:

- The SEM micrographs of the composite specimens show that the $Al_2O_3$, $B_4C$, and SiC particulates are uniformly distributed in all the composite structures and that good interfacial bonding exists between the matrix and the reinforcement elements.
- The hardness, transverse rupture strength, and elongation were affected by the reinforcement particles used in the MMC. The highest hardness, TRS, and elongation were achieved for the Al7039/$Al_2O_3$ composite material. The $Al_2O_3$ particles enhanced the ductility of the Al matrix, resulting in increased bending strength of the specimens. AA7039 reinforced with SiC particles exhibited the worst mechanical properties among the investigated materials.
- The SEM fractographs showed that cracks initiated at the fracture surface of AA7039/$B_4C$ and AA7039/SiC and propagated through the particle–matrix interfaces. No cracks or voids and clear contours were observed in the fracture surface of the AA7039/$Al_2O_3$ composite specimen.
- The machined hole surface quality was affected by the reinforcement elements used in the composite specimens. The AA7039/$Al_2O_3$ composite specimen exhibited better performance than the AA7039 matrix alloy and the AA7039/$B_4C$ and AA7039/SiC composite specimens. The best hole surface roughness was observed for AA7039 reinforced with 10 wt.% $Al_2O_3$ drilled at a spindle speed of 2600 rpm and at a feed rate of 0.12 mm/tooth.
- Better surface quality was obtained at lower feed rates and higher spindle speeds combination, and increasing the feed rates decreased the finished surface quality in the drilling of all specimens.
- The mechanical and microstructural properties of workpiece materials and the drilling parameters, including the cutting speed and feed rate, affected chip formation. Ductile machining with the formation of short chips was achieved in the case of drilling AA7039/$Al_2O_3$ specimens, where the machined surface of the hole remained undamaged. The presence of hard $B_4C$ and SiC particles altered the plastic deformation characteristics of aluminum matrix alloy, resulting in the formation of more fragmented and brittle chips.

## Acknowledgments

The authors wish to thank Hacettepe University Scientific Research Projects Coordination Unit for the financial support with the project number # 014 D05 603 001-636. The authors would like also to thank Poyraz CNC for cutting the mechanical test specimens. Special thanks to ASO technical college and Muzaffer Hasbal for executing the drilling experiments.

## References

[1] Pramanik A, Zhang LC, Arsecularatne JA. Machining of metal matrix composites: effect of ceramic particles on residual stress, surface roughness and chip formation. Int J Mach Tools Manuf 2008;48:1613–25.
[2] El-Gallab M, Sklad M. Machining of Al/SiC particulate metal matrix composites: part II: workpiece surface integrity. J Mater Process Technol 1998;83:277–85.
[3] Bauri R, Surappa MK. Processing and properties of Al–Li–SiCp composites. Sci Technol Adv Mater 2008;8:494–502.
[4] Umanath K, Palanikumar K, Selvamani ST. Analysis of dry sliding wear behaviour of Al6061/SiC/$Al_2O_3$ hybrid metal matrix composites. Compos Part B Eng 2013;53:159–68.
[5] Karabulut Ş. Optimization of surface roughness and cutting force during AA7039/Al2O3 metal matrix composites milling using neural networks and Taguchi method. Measurement 2015;66:139–49.

[6] Ibrahim MF, Ammar HR, Samuel AM, Soliman MS, Almajid A, Samuel FH. Mechanical properties and fracture of Al–15 vol.-%$B_4C$ based metal matrix composites. Int J Cast Met Res 2014;27:7–14.
[7] Ibrahim MF, Ammar HR, Samuel AM, Soliman MS, Samuel FH. On the impact toughness of Al–15 vol.%$B_4C$ metal matrix composites. Compos Part B Eng 2015;79:83–94.
[8] Baradeswaran A, Perumal AE. Study on mechanical and wear properties of Al 7075/$Al_2O_3$/graphite hybrid composites. Compos Part B Eng 2014;56:464–71.
[9] Doel TJA, Bowen P. Tensile properties of particulate-reinforced metal matrix composites. Compos Part A Appl Sci Manuf 1996;27:655–65.
[10] Srivatsan TS. Microstructure, tensile properties and fracture behavior of $Al_2O_3$ particulate-reinforced aluminum alloy metal matrix composites. J Mater Sci 1996;31:1375–88.
[11] Shorowordi KM, Laoui T, Haseeb ASMA, Celis JP, Froyen L. Microstructure and interface characteristics of $B_4C$, SiC and $Al_2O_3$ reinforced Al matrix composites: a comparative study. J Mater Process Technol 2003;142:738–43.
[12] Rajkumar K, Charles JMA, Kumar KV, Praveen JJC, Padmanathan A. Mechanical and machining characteristics of Al/B4C metal matrix composites. Proceedings of the national conference on emerging trends in mechanical engineering, NCETIME 2013.
[13] Ramulu M, Rao PN, Kao H. Drilling of $Al_2O_3$p/6061 metal matrix composites. J Mater Process Technol 2002;124:244–54.
[14] Tosun G, Muratoglu M. The drilling of Al/SiCp metal–matrix composites. Part II: workpiece surface integrity. Compos Sci Technol 2004;64:1413–8.
[15] Basavarajappa S, Chandramohan G, Davim JP. Some studies on drilling of hybrid metal matrix composites based on Taguchi techniques. J Mater Process Technol 2008;196:332–8.
[16] Ahamed AR, Asokan P, Aravindan S, Prakash MK. Drilling of hybrid Al–5% SiCp–5%B4Cp metal matrix composites. Int J Adv Manuf Technol 2010;49:871–7.
[17] Rajmohan T, Palanikumar K, Davim JP. Analysis of surface integrity in drilling metal matrix and hybrid metal matrix composites. J Mater Sci Technol 2012;28:761–8.
[18] Taşkesen A, Kütükde K. Experimental investigation and multi-objective analysis on drilling of boron carbide reinforced metal matrix composites using grey relational analysis. Measurement 2014;47:321–30.
[19] Taskesen A, Kutukde K. Non-contact measurement and multi-objective analysis of drilling temperature when drilling B4C reinforced aluminum composites. Trans Nonferrous Met Soc China 2015;25:271–83.
[20] Halil A. Investigation of influences of pressing pressure and sintering temperature on the mechanical properties of Al–$Al_4C_3$ composite materials. Turk J Eng Environ Sci 2003;27:53–8.
[21] Baradeswaran A, Perumal AE. Influence of B 4 C on the tribological and mechanical properties of Al 7075–$B_4C$ composites. Compos Part B Eng 2013;54:146–52.
[22] Gode C. Mechanical properties of hot pressed SiCp and $B_4C$p/Alumix 123 composites alloyed with minor Zr. Compos Part B Eng 2013;54:34–40.
[23] Kok M. Production and mechanical properties of $Al_2O_3$ particle-reinforced 2024 aluminium alloy composites. J Mater Process Technol 2005;161:381–7.
[24] Shin YC, Dandekar C. Machining of metal matrix composites. 2012.
[25] Rajmohan T, Palanikumar K. Application of the central composite design in optimization of machining parameters in drilling hybrid metal matrix composites. Measurement 2013;46:1470–81.
[26] Manna A, Bhattacharyya B. Investigation for optimal parametric combination for achieving better surface finish during turning of Al/SiC–MMC. Int J Adv Manuf Technol 2004;23:658–65.
[27] Pramanik A, Zhang LC, Arsecularatne JA. An FEM investigation into the behaviour of metal matrix composites: tool–particle interaction during orthogonal cutting. Int J Adv Manuf Technol 2007;47:1497–506.
[28] Pramanik A, Zhang LC, Arsecularatne JA. Micro-indentation of metal matrix composites – an FEM analysis. Key Eng Mater 2007;340–341:563–70.
[29] Hung NP, Yeo SH, Lee KK, Ng KJ. Chip formation in machining particulate-reinforced metal matrix composites. Mater Manuf Process 1998;13:85–100.
[30] Ozcatalbas Y. Chip and built-up edge formation in the machining of in situ $Al_4C_3$–Al composite. Mater Des 2003;24:215–21.